nature methods

BRIEF COMMUNICATION

https://doi.org/10.1038/s41592-020-0926-5



Actin chromobody imaging reveals sub-organellar actin dynamics

Cara R. Schiavon^{1,2,7}, Tong Zhang^{1,7}, Bing Zhao³, Andrew S. Moore⁴, Pauline Wales^{1,2}, Leonardo R. Andrade¹, Melissa Wu¹, Tsung-Chang Sung⁵, Yelena Dayn⁵, Jasmine W. Feng⁶, Omar A. Quintero¹, Gerald S. Shadel², Robert Grosse¹ and Uri Manor¹

The actin cytoskeleton plays multiple critical roles in cells, from cell migration to organelle dynamics. The small and transient actin structures regulating organelle dynamics are challenging to detect with fluorescence microscopy, making it difficult to determine whether actin filaments are directly associated with specific membranes. To address these limitations, we developed fluorescent-protein-tagged actin nanobodies, termed 'actin chromobodies' (ACs), targeted to organelle membranes to enable high-resolution imaging of sub-organellar actin dynamics.

The critical role of the actin cytoskeleton in organelle dynamics is largely accepted but poorly understood. The precise spatiotemporal dynamics of actin at organelle membranes remain particularly unclear due to the combined limitations of currently available actin probes and imaging approaches. For fluorescence microscopy approaches, imaging smaller actin structures in the cell is difficult because the high signal from the dense meshwork of actin filaments throughout the cell overwhelms the signal from the relatively small, transient actin structures associated with organelle dynamics. Furthermore, the limitations in resolution make it difficult to conclude whether any actin filaments are directly associated with the organelle. Here we use fluorescent protein-tagged actin nanobodies, termed ACs1,2, fused to organelle membrane-targeting sequences to facilitate live-cell imaging of sub-organellar actin dynamics with high spatiotemporal resolution. Using these probes, we imaged the spatiotemporal dynamics of mitochondria- and endoplasmic reticulum (ER)-associated actin accumulation at mitochondrial fis-

We hypothesized that AC probes with organelle membrane-targeting sequences could be used to visualize actin filaments closely associated with the target organelle membrane. Given the high mobility of membrane-anchored proteins in a lipid bilayer, an F-actin-binding probe containing only a membrane-anchoring sequence and a fluorescent protein tag should quickly accumulate at sites of F-actin enrichment near the membrane by virtue of its actin-binding activity (Fig. 1a). If there is no F-actin near the membrane, the AC probes freely diffuse throughout the membrane. When F-actin comes close enough to the membrane to bind to the AC probes (approximately 10 nm from the membrane), the AC probes but not the control probes are immobilized at the sites of F-actin accumulation. As actin filaments accumulate, more of the AC probe becomes immobilized. To test this hypothesis,

we generated constructs containing the minimal C-terminal tail membrane-targeting sequences of the yeast Fis1 in the mitochondrial outer membrane or cytochrome b5 in the ER (Cytb5ER), fused to the cytoplasm-facing actin nanobody and the green fluorescent protein tagGFP ('AC-mito' and 'AC-ER')3. Live-cell Airyscan confocal imaging of cells expressing AC-mito or AC-ER counterstained with MitoTracker dye revealed specific regions of AC-mito accumulation on the mitochondrial surfaces, with similar results for AC-ER on the ER (Fig. 1b and Supplementary Videos 1-4). To rule out the possibility that the membrane-targeting sequences we used were causing the probe to accumulate in specific regions independent of actin-binding activity, we cotransfected AC-mito or AC-ER with control probes: mCherry-tagged mitochondrial (Fis1) and ER (Cytb5ER) membrane-targeting sequences (mCherry-mito and mCherry-ER). As expected, the mCherry-mito and mCherry-ER signals were evenly distributed along their respective organelle membranes, with no obvious accumulation in any specific regions. In contrast, the coexpressed AC-mito and AC-ER constructs displayed significant accumulation in specific regions on their respective organelles (Fig. 1b), as quantified by the coefficient of variance (Methods). Cells expressing AC-ER counterstained with MitoTracker revealed high AC-ER accumulation at ER-mitochondria contact sites compared to the mCherry-ER control probe (Fig. 1b, Extended Data Fig. 1 and Supplementary Videos 3 and 4). Overall, AC probe labeling appears to provide both more specificity and sensitivity than phalloidin staining for identifying organelle-associated actin (Extended Data Fig. 2). Importantly, there was no detected increase in organelle-associated actin in cells expressing the AC probes (Extended Data Fig. 2c). Similarly, we found no change in endogenous Fis1 localization to mitochondria in AC-mito-expressing cells (Extended Data Fig. 3). Using a different membrane-targeting sequence (Cytb5mito3) and/or a different F-actin probe (LifeAct4) yielded similar results (Extended

Fluorescence recovery after photobleaching (FRAP) experiments showed that both the AC and mCherry control probes were highly mobile on the membrane, but only the AC probes exhibited lower mobility at sites of AC specific accumulation (Fig. 1c, Extended Data Fig. 5 and Supplementary Videos 5 and 6). However, the AC probe mobility was similar to that of the control probes in diffuse regions lacking AC accumulation (Extended Data Fig. 5), consistent with the model in which AC accumulation is indicative

'Waitt Advanced Biophotonics Center, Salk Institute for Biological Studies, La Jolla, CA, USA. ²Molecular and Cellular Biology Laboratory, Salk Institute for Biological Studies, La Jolla, CA, USA. ³Institute of Experimental and Clinical Pharmacology and Toxicology, University of Freiburg, Freiburg im Breisgau, Germany. ⁴Janelia Research Campus, Howard Hughes Medical Institute, Chevy Chase, MD, USA. ⁵Transgenic Core, Salk Institute for Biological Studies, La Jolla, CA, USA. ⁶Department of Biology, University of Richmond, Richmond, VA, USA. ⁷These authors contributed equally: Cara R. Schiavon, Tong Zhang.

[™]e-mail: umanor@salk.edu

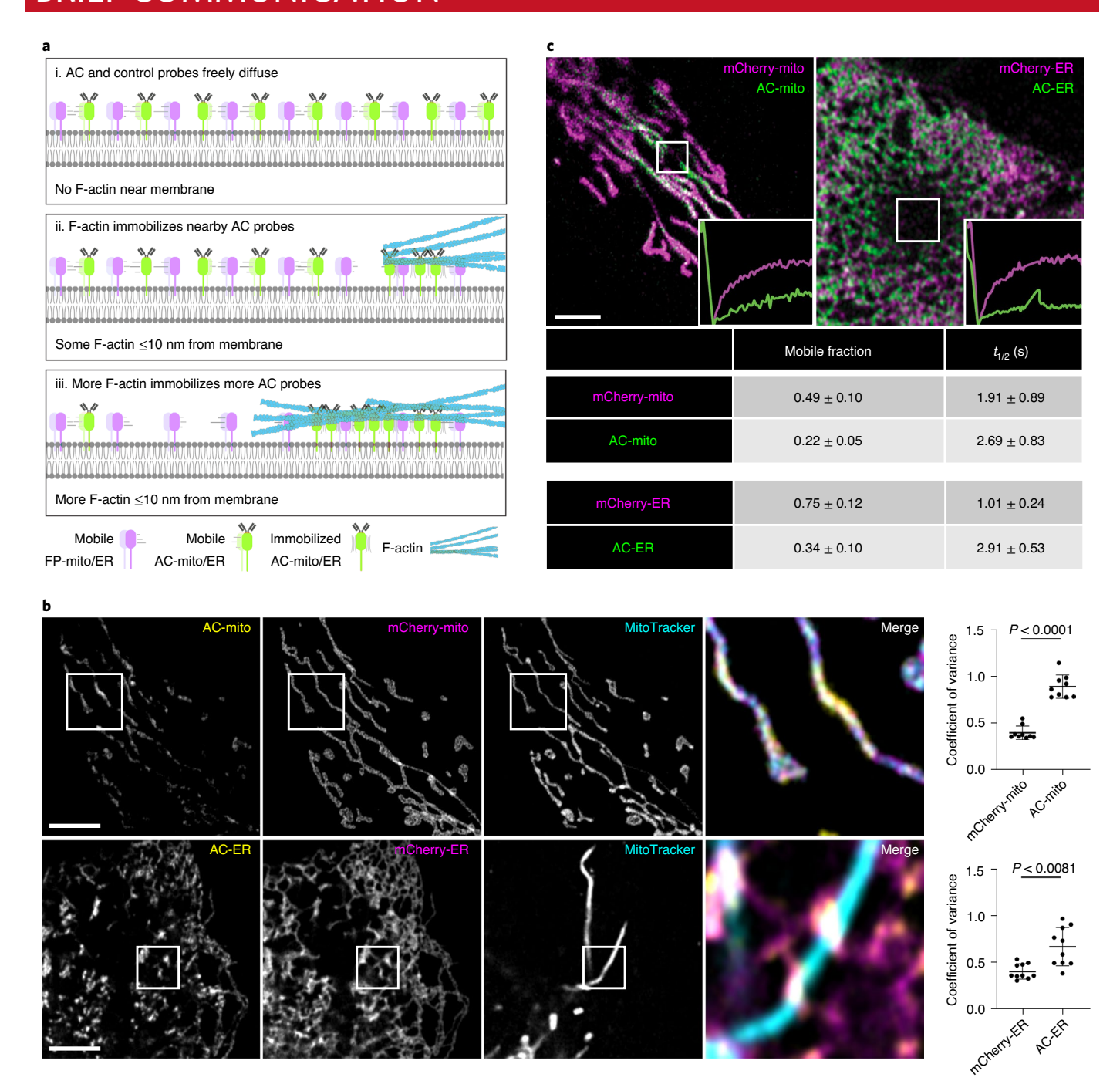


Fig. 1 Mitochondria- and ER-targeted ACs reveal sub-organellar F-actin-associated domains. **a**, Cartoon model of changes in organelle membrane-targeted AC probe localization in response to the presence of F-actin. **b**, Coexpression of mCherry-tagged control probes and AC probes in U2OS cells. Sub-organellar accumulation was observed in all cells imaged (AC-mito, n = 68 cells; AC-ER, n = 55 cells). Scale bars, $5 \mu m$. Sub-organellar accumulation was quantified as the coefficient of variance within the mitochondrial (n = 9 cells) or ER (n = 10 cells) area (Methods). P values were determined using a two-tailed paired ratio t-test. These results were reproducible across nine independent experiments. **c**, FRAP of cells coexpressing AC and control probes (AC, n = 10 cells; mCherry control, n = 14 cells). The table displays the average mobile fraction and the half-time to recovery $t_{1/2} \pm s.d.$ These results were reproducible across four independent experiments.

of immobilization by F-actin-binding activity (Fig. 1a)^{5,6}. To further test whether sub-organellar AC accumulation was dependent on F-actin, we treated AC-expressing cells with the F-actin depolymerizing drug latrunculin B, which significantly reduced sub-organellar accumulation and increased the mobility of the AC probes (Extended Data Fig. 6). Taken together, these results strongly support the conclusion that AC probe accumulation and mobility is

dependent on F-actin, yet the AC binding dynamics are still relatively fast compared to actin filament turnover rates⁷.

Given their high mobility, we hypothesized that AC probes would reveal dynamic changes in F-actin (dis)assembly on their respective organelles. In HeLa cells, F-actin 'waves' cycle around the cell, decorating subpopulations of mitochondria before their fission and subsequent fusion⁸. As expected, we found co-accumulation of F-actin

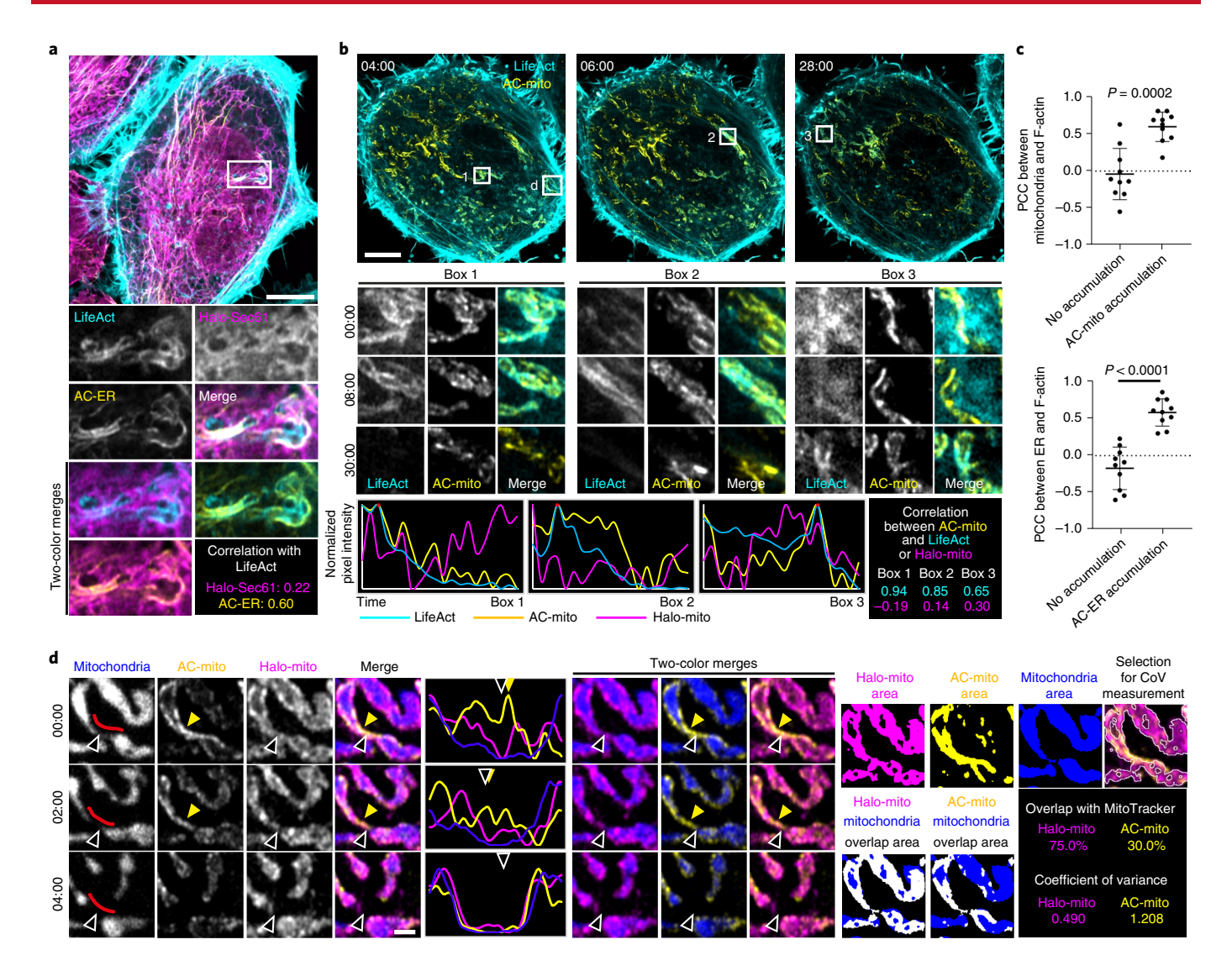


Fig. 2 | AC-mito and AC-ER dynamically label mito- and ER-associated actin. a, A HeLa cell coexpressing LifeAct, AC-ER and the Halo-ER control probe. An area of actin and AC-ER co-accumulation (white box) is shown in the high-magnification images. Pearson's correlation coefficient values for LifeAct:Halo-ER and LifeAct:AC-ER are shown. Scale bar, 5 μm. These results were reproducible across 12 independent experiments. b, An actin wave cycling around the cell was imaged in HeLa cells coexpressing LifeAct, AC-mito, Halo-mito control and blue fluorescent protein (BFP)-mito. Only LifeAct and AC-mito are shown for simplicity. Boxes 1-3 mark regions of LifeAct accumulation at different time points. Box 'd' marks the area shown at higher magnification in d. Scale bar, 5 μm. Graphs show the change in LifeAct, AC-mito and Halo-mito control pixel intensity in the boxed regions over time. The correlation between AC-mito:LifeAct and AC-mito:Halo-mito pixel intensity over time for each boxed region is shown. These results were reproducible across four independent experiments. c, Cells were either cotransfected with AC-mito and LifeAct and stained with MitoTracker (top graph) or cotransfected with AC-ER, LifeAct and the mCherry-ER control probe (bottom graph). Pearson's correlation coefficient was calculated between mitochondria:LifeAct (top graph) or ER:LifeAct (bottom graph) in regions showing AC probe accumulation; n=10 cells per condition. P values were determined using a two-tailed Welch's t-test. d, A higher magnification of Box 'd' from b shows mitochondria (BFP-mito), the Halo-mito control probe and the AC-mito signal during a mitochondrial fission event. Red lines indicate the mitochondrial region used to generate the line scan. Arrows mark the site of mitochondrial fission (hollow) and regions of AC-mito accumulation (yellow). Example images of the areas used to determine the degree of mitochondria overlap and coefficient of variance values for Halo-mito and AC-mito and the resulting values are shown on the right.

and AC probes (but not the control probes) on specific regions of the organelles (Fig. 2). Time-lapse imaging of cells labeled with LifeAct, the AC probes and a mitochondrial matrix marker revealed fluctuations in actin accumulation on mitochondrial subpopulations as actin waves cycled throughout the cell (Fig. 2b, Extended Data Fig. 7 and Supplementary Videos 7–9). Fluorescence intensity changes in AC probe levels matched those of LifeAct, and mitochondrial fission occurred after actin accumulation, as previously reported (Fig. 2d and Supplementary Video 10). The wave

cycling rates matched those of cells not expressing AC probes, and neighboring cells expressing varying levels of AC probes also had matching rates. Increased AC accumulation around fragmented mitochondria induced by ionomycin treatment was also evident. There was no difference in the rate of ionomycin-induced mitochondrial fragmentation in cells expressing AC probes compared to neighboring untransfected cells (Extended Data Fig. 8 and Supplementary Videos 11 and 12). Overall, these results show that AC probes reliably label dynamic actin (dis)assembly without

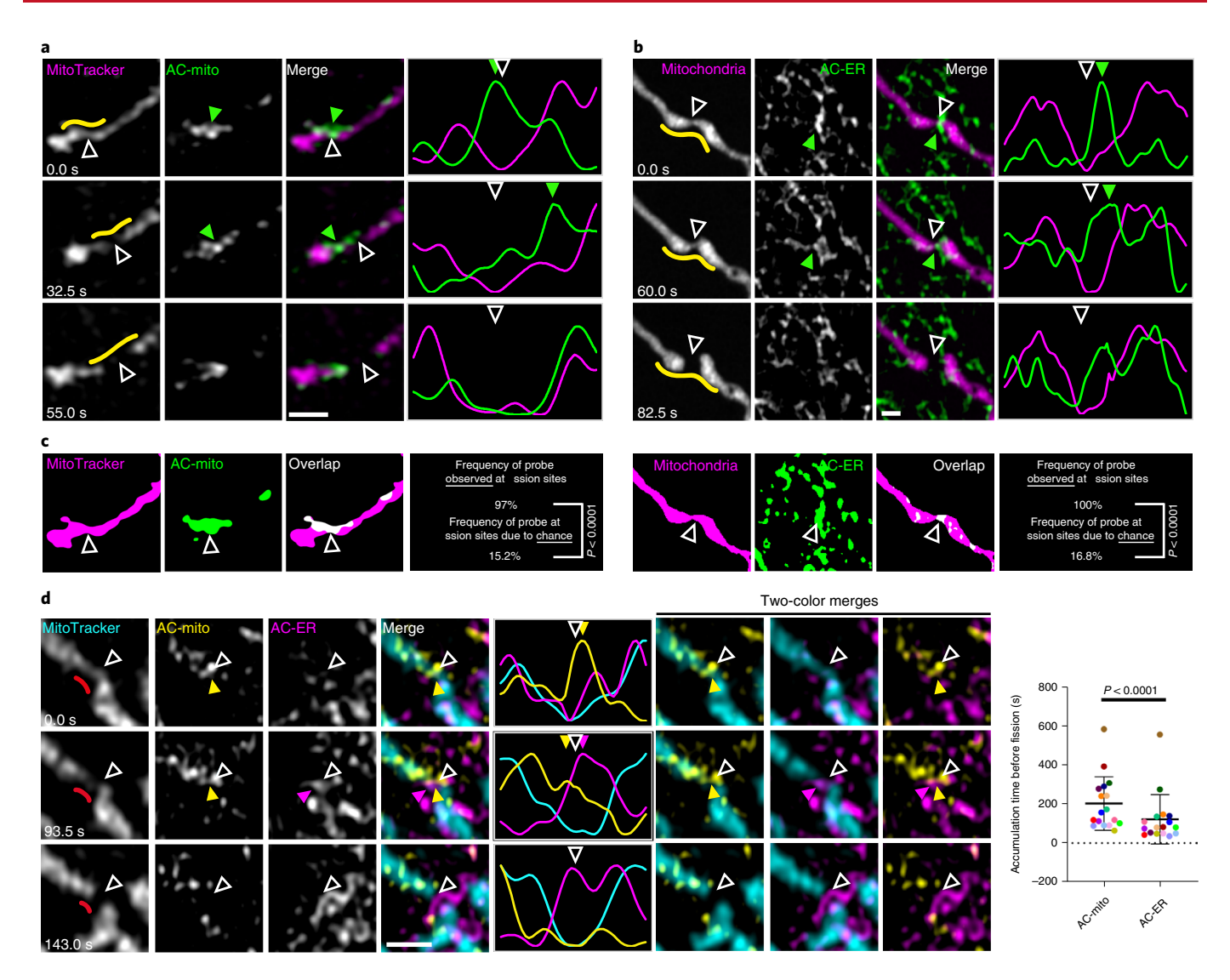


Fig. 3 | Mitochondria- and ER-associated actin accumulates before mitochondrial fission. a,b, A mitochondrial fission event from a HeLa cell expressing AC-mito (**a**) or coexpressing BFP-mito and AC-ER (**b**) and stained with MitoTracker. Arrows mark the site of mitochondrial fission (hollow) and AC-mito accumulation (green). Yellow lines indicate the area used to generate the line scan. Scale bar, 1μm. These results were reproducible across 21 independent experiments. **c**, Examples of AC probe areas used to determine that accumulation at mitochondrial fission sites was not due to chance. Images show the mitochondria and AC probe areas generated by the images from the first time points in **a** and **b**. The frequency of the AC probes observed at fission sites (AC-mito: 32 of 33 fission events; AC-ER: 31 of 31 fission events) was compared to the frequency that would be expected by chance (Methods). *P* values were determined by Fisher's exact test. **d**, A mitochondrial fission event from a HeLa cell coexpressing AC-mito and AC-ER and stained with MitoTracker. Arrows mark the site of mitochondrial fission (hollow), AC-mito accumulation (yellow) and AC-ER accumulation (magenta). Red lines mark the area used to the generate the line scan. Scale bar, 1μm. This order of events is consistently observed and quantified in the scatterplot. Each dot color corresponds to an individual fission event (*n*=17). *P* values were determined by a two-tailed ratio paired *t*-test. These results were reproducible across seven independent experiments.

altering the kinetics or mitochondrial behavior in normal or stressed conditions.

Previous studies demonstrated a role for actin in driving mitochondrial fission at ER-mitochondria contact sites, likely with actin playing a role in force generation and Drp1 recruitment and activation⁹⁻¹⁶. To determine the kinetics of mitochondria-and ER-associated actin accumulation at mitochondrial fission sites, we performed live imaging of cells expressing AC-mito and AC-ER counterstained with MitoTracker. Mitochondrial fission sites displayed accumulation of both AC-mito and AC-ER before Drp1- and ER-mediated fission (Fig. 3, Extended Data Figs. 9 and 10, Supplementary Figs. 1–8 and Supplementary Videos 13–19). Approximately 5% of cells transfected with AC-mito expressed

with a CMV promoter displayed overexpression artifacts (that is, increased clustering and reduced mobility of mitochondria; Supplementary Video 20). To address this, we expressed AC-mito using a ubiquitin UbC promoter; this dramatically reduced the prevalence of overexpression artifacts (<0.01% of transfected cells). We did not detect a change in mitochondrial membrane potential, fission rate or ER-mitochondria contacts in cells expressing the AC probes (Extended Data Fig. 9). In cells expressing both AC-mito and AC-ER, we invariably observed AC-mito accumulation before AC-ER accumulation (Fig. 3d, Supplementary Fig. 9 and Supplementary Video 21).

Membrane-anchored AC probes provide a new tool for studying membrane-associated actin dynamics with much higher effective

NATURE METHODS

BRIEF COMMUNICATION

resolution than cytoplasmic actin probes. In addition to the plasma membrane ^{17,18}, the variety of subcellular compartments, protein targets and corresponding subcellular or sub-organellar processes that can be studied will increase as additional nanobodies or other kinds of protein-binding motifs and subcellular membrane-targeting sequences are developed. In addition, future studies that switch the fluorescent markers for probes compatible with electron microscopy, and/or proximity markers for downstream mass spectrometry analyses such as APEX2 (ref. ¹⁹) or TurboID²⁰, will likely reveal new insights into fundamental processes and molecular mechanisms in actin and organelle cell biology.

Online content

Any methods, additional references, Nature Research reporting summaries, source data, extended data, supplementary information, acknowledgements, peer review information; details of author contributions and competing interests; and statements of data and code availability are available at https://doi.org/10.1038/s41592-020-0926-5.

Received: 3 July 2019; Accepted: 15 July 2020; Published online: 10 August 2020

References

- Rocchetti, A., Hawes, C. & Kriechbaumer, V. Fluorescent labelling of the actin cytoskeleton in plants using a cameloid antibody. *Plant Methods* 10, 12 (2014).
- Melak, M., Plessner, M. & Grosse, R. Actin visualization at a glance. J. Cell Sci. 130, 525–530 (2017).
- Rapaport, D. Finding the right organelle. Targeting signals in mitochondrial outer-membrane proteins. EMBO Rep. 4, 948–952 (2003).
- Riedl, J. et al. Lifeact: a versatile marker to visualize F-actin. Nat. Methods 5, 605–607 (2008).
- Sprague, B. L. & McNally, J. G. FRAP analysis of binding: proper and fitting. Trends cell Biol. 15, 84–91 (2005).
- Sprague, B. L., Pego, R. L., Stavreva, D. A. & McNally, J. G. Analysis of binding reactions by fluorescence recovery after photobleaching. *Biophys. J.* 86, 3473–3495 (2004).

- Panza, P., Maier, J., Schmees, C., Rothbauer, U. & Sollner, C. Live imaging of endogenous protein dynamics in zebrafish using chromobodies. *Development* 142, 1879–1884 (2015).
- Moore, A. S., Wong, Y. C., Simpson, C. L. & Holzbaur, E. L. Dynamic actin cycling through mitochondrial subpopulations locally regulates the fission– fusion balance within mitochondrial networks. *Nat. Commun.* 7, 12886 (2016).
- Manor, U. et al. A mitochondria-anchored isoform of the actin-nucleating spire protein regulates mitochondrial division. eLife 4, e08828 (2015).
- Chakrabarti, R. et al. INF2-mediated actin polymerization at the ER stimulates mitochondrial calcium uptake, inner membrane constriction and division. *J. Cell Biol.* 217, 251–268 (2018).
- Korobova, F., Ramabhadran, V. & Higgs, H. N. An actin-dependent step in mitochondrial fission mediated by the ER-associated formin INF2. *Science* 339, 464-467 (2013).
- Korobova, F., Gauvin, T. J. & Higgs, H. N. A role for myosin II in mammalian mitochondrial fission. Curr. Biol. 24, 409–414 (2014).
- Yang, C. & Svitkina, T. M. Ultrastructure and dynamics of the actin-myosin II cytoskeleton during mitochondrial fission. *Nat. Cell Biol.* 21, 603–613 (2019).
- De Vos, K. J., Allan, V. J., Grierson, A. J. & Sheetz, M. P. Mitochondrial function and actin regulate dynamin-related protein 1-dependent mitochondrial fission. *Curr. Biol.* 15, 678–683 (2005).
- Li, S. et al. Transient assembly of F-actin on the outer mitochondrial membrane contributes to mitochondrial fission. *J. Cell Biol.* 208, 109–123 (2015).
- Ji, W. K., Hatch, A. L., Merrill, R. A., Strack, S. & Higgs, H. N. Actin filaments target the oligomeric maturation of the dynamin GTPase Drp1 to mitochondrial fission sites. eLife 4, e11553 (2015).
- Shirai, Y. M. et al. Cortical actin nodes: their dynamics and recruitment of podosomal proteins as revealed by super-resolution and single-molecule microscopy. PLoS ONE 12, e0188778 (2017).
- Bisaria, A., Hayer, A., Garbett, D., Cohen, D. & Meyer, T. Membrane-proximal F-actin restricts local membrane protrusions and directs cell migration. *Science* 368, 1205–1210 (2020).
- Lam, S. S. et al. Directed evolution of APEX2 for electron microscopy and proximity labeling. Nat. Methods 12, 51–54 (2015).
- Branon, T. C. et al. Efficient proximity labeling in living cells and organisms with TurboID. Nat. Biotechnol. 36, 880–887 (2018).

Publisher's note Springer Nature remains neutral with regard to jurisdictional claims in published maps and institutional affiliations.

 $\ensuremath{\texttt{@}}$ The Author(s), under exclusive licence to Springer Nature America, Inc. 2020

Methods

Cell culture. U2OS, HeLa and Hap1 cells were purchased from the American Type Culture Collection (ATCC). HeLa cells stably expressing LifeAct-mCherry were a gift from the Wedlich-Soldner laboratory $^{\!\!\!\!\!\!^{11}}$. Cells were grown in DMEM supplemented with 10% FBS at 37 °C with 5% $\rm CO_2$. Cells were transfected with Lipofectamine 2000 (Thermo Fisher). Cells were plated onto either 8-well no. 1.5 imaging chambers or no. 1.5 35-mm dishes (Cellvis) that were coated with $10\,\mu g$ ml $^{\!\!\!-1}$ fibronectin in PBS at 37 °C for 30 min before plating. MitoTracker Deep Red (50 nM; Thermo Fisher) was added to cells for 30 min, and then cells washed for at least 30 min to allow for recovery time before imaging in FluoroBrite (Thermo Fisher) medium.

Airyscan confocal imaging. Cells were imaged with a Plan-Apochromat $\times 63/1.4\,\mathrm{NA}$ oil objective on an inverted Zeiss 880 LSM Airyscan confocal microscope with the environmental control system supplying 37 °C, 5% CO $_2$ and humidity for live-cell imaging. The GFP channels were imaged with a 488-nm laser line at $\sim\!500$ -nW laser power. The mCherry or tagRFP channels were imaged with a 561-nm laser at $\sim\!1$ - μ W laser power. The MitoTracker Deep Red channel was imaged with $\sim\!250$ -nW laser power. For time-lapse imaging, the zoom factor was set between 3× and 6× to increase the frame rate. In all cases, the maximum pixel-dwell time ($\sim\!0.684\,\mu\mathrm{s}$ per pixel) and 2× Nyquist optimal pixel size ($\sim\!40\,\mathrm{nm}$ per pixel) was used.

Spinning disk confocal imaging. Cells were imaged with a Plan-Apochromat $\times 40/1.3\,\mathrm{NA}$ oil objective on a Zeiss CSU spinning disk confocal microscope with a CSU-X1 Yokogawa spinning disk scan head on a Prime 95B sCMOS camera (Teledyne Photometrics). The 488-nm, 561-nm and 647-nm laser powers were set at 100 μ W, 200 μ W and 20 μ W with 300-ms, 300-ms and 150-ms exposure times, respectively.

Antibodies. We used the rabbit anti-Fis1 antibody against the N-terminal cytoplasmic facing side of the human Fis1 protein (Prestige Antibodies Powered by Atlas Antibodies; Sigma-Aldrich, HPA017430). The amino acid sequence of the antigen is MEAVLNELVSVEDLLKFEKKFQSEKAAGSVSKSTQFEYAWCLV-RSKYNDDIRKGIVLLEELLPKGS

 $\label{eq:keeq} \textbf{KEEQRDYVFYLAVGNYRLKEYEKALKYVRGLLQTEPQNNQAKELERLID} \\ \textbf{KAMKKD}.$

Immunofluorescence. Cells were washed in PBS and then fixed with 4% paraformaldehyde for 30 min before permeabilization with 0.1% Triton-X100 for 30 min. Cells were then blocked overnight with 4% BSA at 4 °C. Cells were incubated with primary antibody for 2 h, rinsed 3× with PBS for 10 min each and then incubated with secondary antibodies (Jackson Immunoresearch Laboratories) for 1 h. Next, cells were rinsed 3× with PBS for 10 min each, counterstained with Alexa Fluor 405 phalloidin (Thermo Fisher) for 30 min, rinsed with PBS 3× for 10 min each and then mounted with ProLong Glass antifade reagent (Thermo Fisher).

Image processing and analysis. After acquisition, images were Airyscan processed using the auto-filter 2D-SR settings in Zen Blue (ZEISS). All images were post-processed and analyzed using Imaris (BITPLANE) and Fiji software²². All images shown are from single focal planes unless stated otherwise.

Data quantification and statistics. All line scans were normalized and plotted in Microsoft Excel. All statistical analyses and graphs were generated using GraphPad Prism 8 software. All graphs display horizontal lines marking average values and error bars indicate s.d.

AC probe 'accumulation' calculation. Using Fiji, a square selection was drawn around a region with obvious AC probe accumulation (1.5 μm^2 for mitochondria and 0.6 μm^2 for ER). The mean pixel intensity of the AC and mCherry control probes within the selection was measured. Another square of equal dimensions was drawn in an adjacent area with mCherry signal but without obvious AC probe accumulation. Mean pixel intensity was also measured in this region. The mean pixel intensity in the accumulated region was then divided by the mean pixel intensity in the region without accumulation (Extended Data Fig. 5).

Determination of coefficient of variance. We measured the extent of sub-organellar accumulation by quantifying the coefficient of variance as follows: In Fiji, the mCherry-mito or mCherry-ER signal was used to generate a mask of the mitochondria or ER, respectively. A selection was generated based on this mask (Fig. 2d and Extended Data Fig. 10a). The mean pixel intensity and s.d. within the mask were measured. The coefficient of variance was determined by dividing the s.d. by the mean pixel intensity.

Determination of percentage overlap. Masks of ER, mitochondria, actin and AC and mCherry probes were generated in Fiji. For AC probes, thresholding was set to mask only the top 25% of AC probe signal based on maximum pixel intensity (see the 'clipped' panels in Supplementary Fig. 2). All other masks were generated using default thresholding settings in Fiji, which uses the IsoData algorithm developed by Ridler and Calvard²³. The integrated density of each mask was calculated.

Areas of overlap between masks were generated using the image calculator tool in Fiji, and the integrated density of these areas was also measured. These values were used to calculate the percentage overlap (that is, integrated density for area of overlap between AC-mito and mitochondria divided by integrated density for mitochondrial area yields the percentage of mitochondria overlapped by AC-mito). This percentage was interpreted as the probability of AC probes localizing to fission sites by chance (Fig. 3c).

Colocalization analysis. Pearson's correlation coefficient was determined using the Coloc 2 plugin in Fiji (https://imagej.net/Coloc_2/). For analysis of colocalization in regions with or without AC probe accumulation (Fig. 2c), a square selection was drawn around a region with obvious AC probe accumulation and an equal-sized square was drawn in an adjacent region without AC probe accumulation. Square sizes were $1.5\,\mu\text{m}^2$ for AC-mito analysis and $0.6\,\mu\text{m}^2$ for AC-ER analysis. For mitochondria–ER contact analysis (Extended Data Fig. 9c), a peripheral region (98.5 μm^2) of the cell containing mitochondria and ER was selected. This was done to prevent artificially high values resulting from the large amount of ER and mitochondria overlap typically observed in the perinuclear region, which is too dense to resolve by Airyscan confocal microscopy.

FRAP analysis. FRAP experiments were performed on a Zeiss 880 Airyscan confocal microscope using a Plan-Apochromat 63x/1.4 Oil DIC objective. Transfected cells were maintained at 37 °C with 5% CO₂ in FluoroBrite DMEM (Gibco) and 10% FBS (VWR) culture medium. The 488-nm and 561-nm excitation laser lines and Airyscan detectors were driven by Zeiss Zen Black software. FRAP experiments were done in one focal plane, using the following conditions: three pre-bleach frames were acquired at maximum speed with a 488-nm laser at 25-μW power and a 561-nm laser at 13-μW power. The photobleaching of selected regions was performed with a 488-nm laser at 5-mW power at maximum speed for 30 iterations. The post-bleach acquisition was performed with a 488 nm laser at pre-bleach imaging settings for 100 frames. The fluorescence intensity of the acquired images was quantified in Fiji following the principles outlined by Lippincott-Schwartz et al. 24. The mobile fraction was determined as the percentage of fluorescence recovery at full recovery. The $t_{1/2}$ was determined as the time taken for the fluorescence intensity in the bleached region to recover to 50% of the full recovery value after bleaching. If objects moved in or out of the region of interest during the recovery phase, they were not included in our analyses.

Actin wave pixel-intensity measurements. Square selections were made in Fiji (three selections per cell), and the mean pixel intensity was measured over time. The selections used were $10.1\,\mu\text{m}^2$ for data collected using Airyscan confocal and $32.8\,\mu\text{m}^2$ for data collected using spinning disk confocal microscopy.

Mitochondrial membrane potential. The mean threshold value for each cell was obtained through thresholding to include mitochondria using the MitoTracker Deep Red channel. The average pixel intensity in the thresholded region was measured. The relative intensity for each cell was then calculated by dividing the mean threshold value for each cell by the average mean threshold value of all untransfected cells within the same image. The relative signal intensity of each transfected and untransfected cell was then plotted and graphed.

Plasmids. Drp1-mCherry was a kind gift from G. Voeltz (Addgene plasmid no. 49152), and mCherry-Cytob₃RR was a gift from N. Borgese²⁵. Halo-Sec61 (ref. ²⁶), Halo-Fis1 (Addgene plasmid no. 111136), LifeAct-mScarlet (Addgene plasmid no. 85054) and mTagBFP2-mito²⁷ used for the experiments shown in Fig. 2 were gifts from the Lippincott-Schwartz laboratory. All custom actin nanobody probes were generated starting from the commercial vector of AC-tagGFP or AC-tagRFP (ChromoTek) and cloned via the BgIII and NotI restriction sites. The following amino acid sequences were attached to the C-terminal portion of the AC probes to target the protein either to mitochondria or the ER:

Fis1 (AC-mito and LifeAct-GFP-Fis1):

IQKETLKGVVVAGGVLAGAVAVASFFLRNKRR³

Cytb5mito ('Cyto b_5 RR') (AC-GFP-Cytb5mito and LifeAct-GFP-Cytb5mito): FEPSETLITTVESNSSWWTNWVIPAISALVVALMYRR²5

Cytb5ER (AC-ER):

IDSSSSWWTNWVIPAISAVAVALMYRLYMAED³

LifeAct-GFP-Fis1, LifeAct-GFP-Cytb5mito and AC-GFP-Cytb5mito were generated using PFU Ultra II for megaprimer PCR insertion²⁸. The PCR primers, intended modifications, insert templates and destination plasmids are listed in Supplementary Table 1. All constructs were sequenced completely across their coding region.

Reporting Summary. Further information on research design is available in the Nature Research Reporting Summary linked to this article.

Data availability

The original source data for quantification and the raw imaging data used for all the presented figures and videos are available from https://doi.org/10.5281/zenodo.2851619/. Source data are provided with this paper.

BRIEF COMMUNICATION

References

- Wales, P. et al. Calcium-mediated actin reset (CaAR) mediates acute cell adaptations. eLife 5, e19850 (2016).
- Schindelin, J. et al. Fiji: an open-source platform for biological-image analysis. Nat. Methods 9, 676–682 (2012).
- 23. Ridler, T. & Calvard, S. Picture thresholding using an iterative selection method. *IEEE Trans. Syst. Man Cybern.* **8**, 630–632 (1978).
- Lippincott-Schwartz, J., Snapp, E. L. & Phair, R. D. The development and enhancement of FRAP as a key tool for investigating protein dynamics. *Biophys. J.* 115, 1146–1155 (2018).
- Borgese, N., Gazzoni, I., Barberi, M., Colombo, S. & Pedrazzini, E. Targeting
 of a tail-anchored protein to endoplasmic reticulum and mitochondrial outer
 membrane by independent but competing pathways. *Mol. Biol. Cell* 12,
 2482–2496 (2001).
- Omari, S. et al. Noncanonical autophagy at ER exit sites regulates procollagen turnover. Proc. Natl Acad. Sci. USA 115, E10099–E10108 (2018).
- Subach, O. M., Cranfill, P. J., Davidson, M. W. & Verkhusha, V. V. An enhanced monomeric blue fluorescent protein with the high chemical stability of the chromophore. *PLoS ONE* 6, e28674 (2011).
- Geiser, M., Cebe, R., Drewello, D. & Schmitz, R. Integration of PCR fragments at any specific site within cloning vectors without the use of restriction enzymes and DNA ligase. *BioTechniques* 31, 88–90 (2001).

Acknowledgements

We are grateful to S. Harada (Salk Institute for Biological Studies) for help with the cartoon diagram for Fig. 1. We thank C. Obara and J. Lippincott-Schwartz (Janelia Farms) for critical feedback and suggestions on the manuscript. This work was also greatly improved by feedback on our initial bioRxiv preprint received via Twitter. The Waitt Advanced Biophotonics Center is funded by the Waitt Foundation and Core Grant application National Cancer Institute (NCI) Cancer Center Support Grant (CCSG; CA014195). This work was supported by the Transgenic Core Facility of the Salk

Institute with funding from the National Institutes of Health (NIH)–NCI CCSG (P30 014195). The laboratory of R.G. is funded by grants from the Human Frontier Science Program (HFSP; RGP0021/2016) and the Cluster of Excellence Centre for Integrative Biological Signaling Studies (CIBSS; EXC-2189). G.S.S. is supported by a NIH grant (no. R01 AR069876) and the Salk Institute Audrey Geisel Chair in Biomedical Science. The laboratory of O.A.Q. is supported by a National Institute of General Medical Sciences grant (NIGMS; R15 GM119077) and funding from the University of Richmond School of Arts & Sciences.

Author contributions

C.R.S., T.Z., B.Z., O.A.Q., G.S.S., R.G. and U.M. planned the experimental design and data analysis; C.R.S., T.Z., A.S.M., L.R.A., M.W., J.W.F. and U.M. performed the experiments; C.R.S., T.Z., A.S.M., P.W. and J.W.F. performed data analysis and quantification; B.Z., T.C.S., Y.D., O.A.Q., G.S.S. and R.G. provided key reagents; U.M. supervised the study; and C.R.S., T.Z. and U.M. composed the figures and videos and wrote the manuscript with input from the rest of the authors.

Competing interests

The authors declare no competing interests.

Additional information

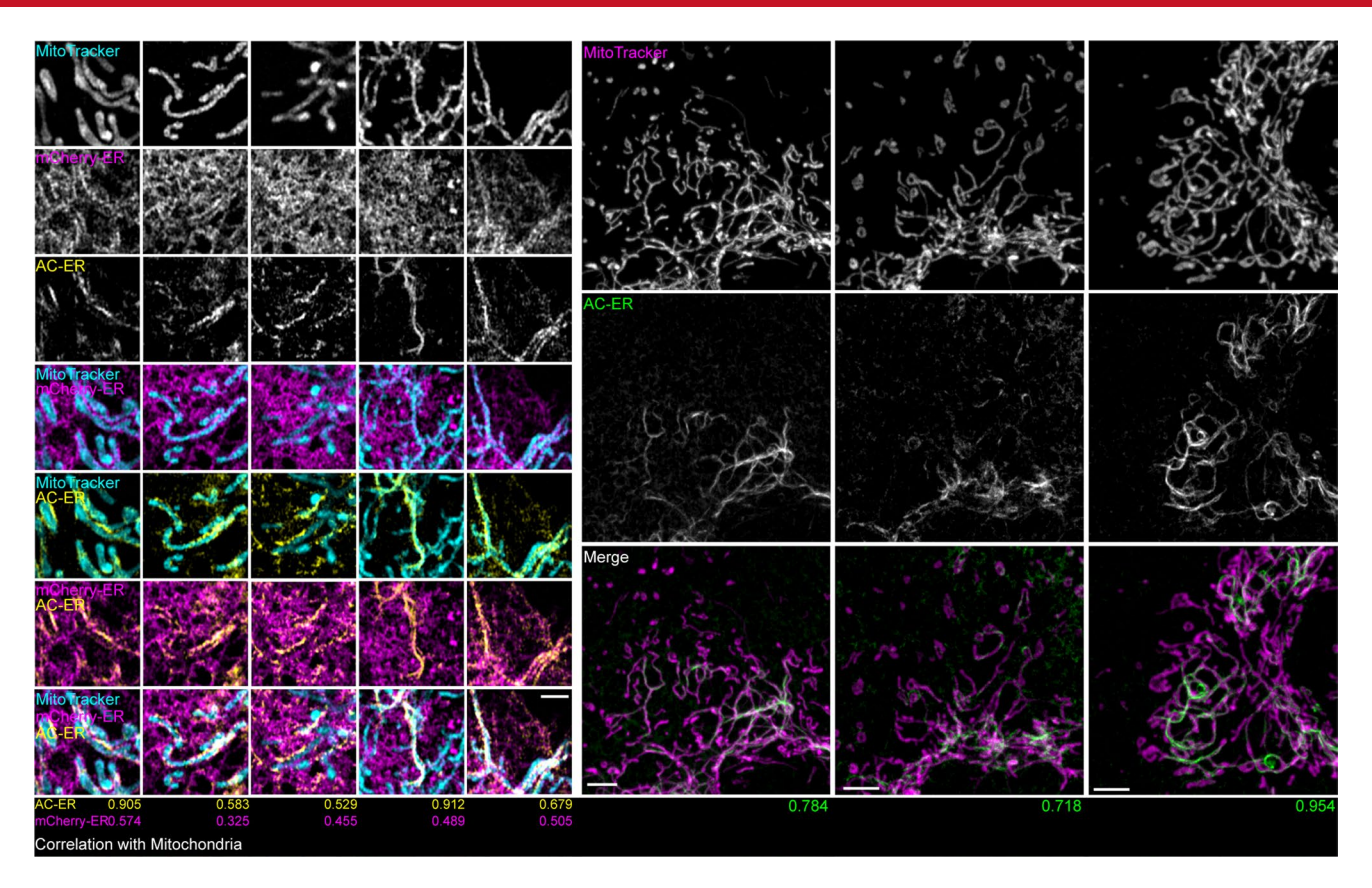
Extended data is available for this paper at https://doi.org/10.1038/s41592-020-0926-5.

Supplementary information is available for this paper at https://doi.org/10.1038/s41592-020-0926-5.

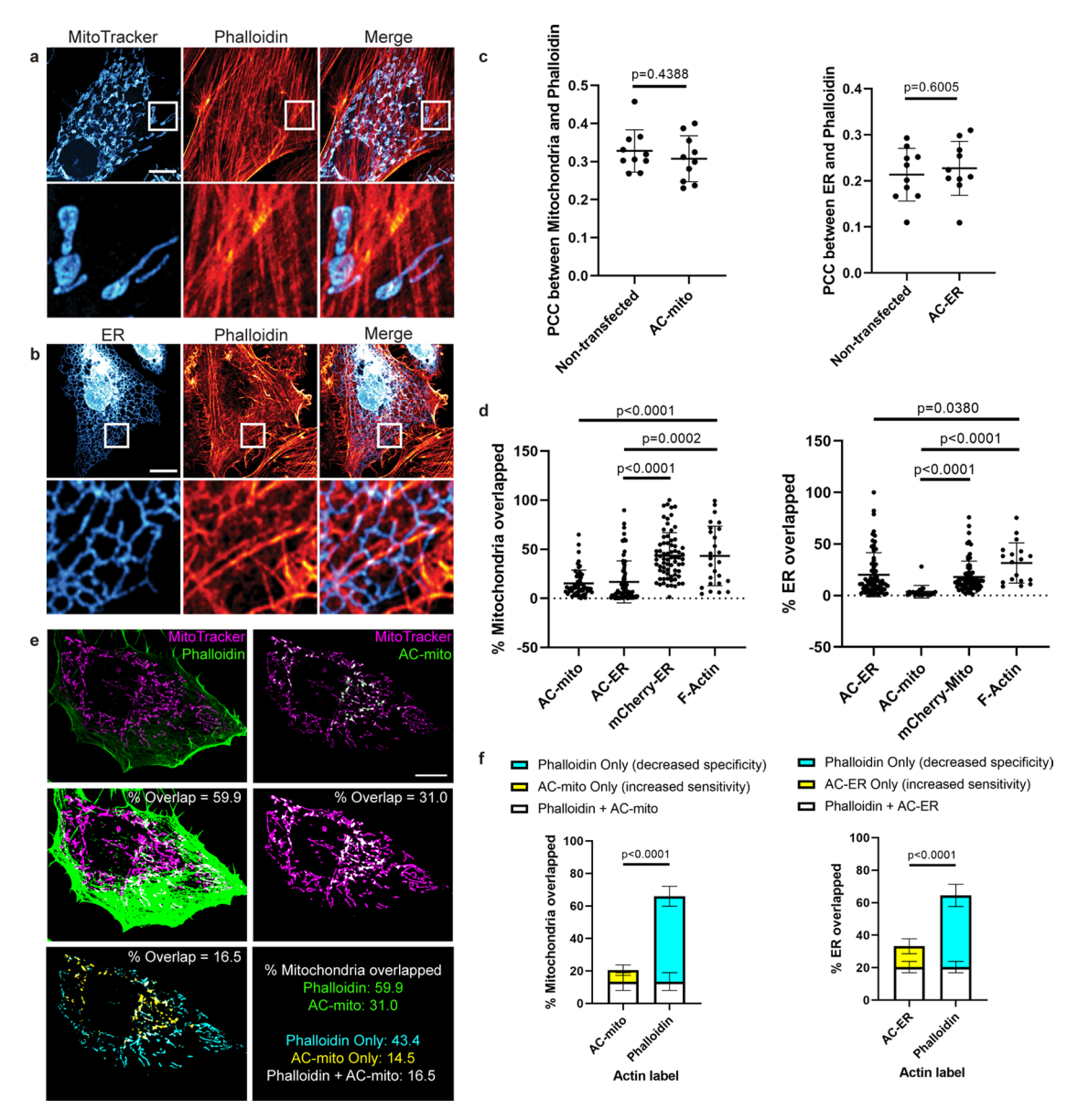
Correspondence and requests for materials should be addressed to U.M.

Peer review information Rita Strack was the primary editor on this article and managed its editorial process and peer review in collaboration with the rest of the editorial team.

Reprints and permissions information is available at www.nature.com/reprints.

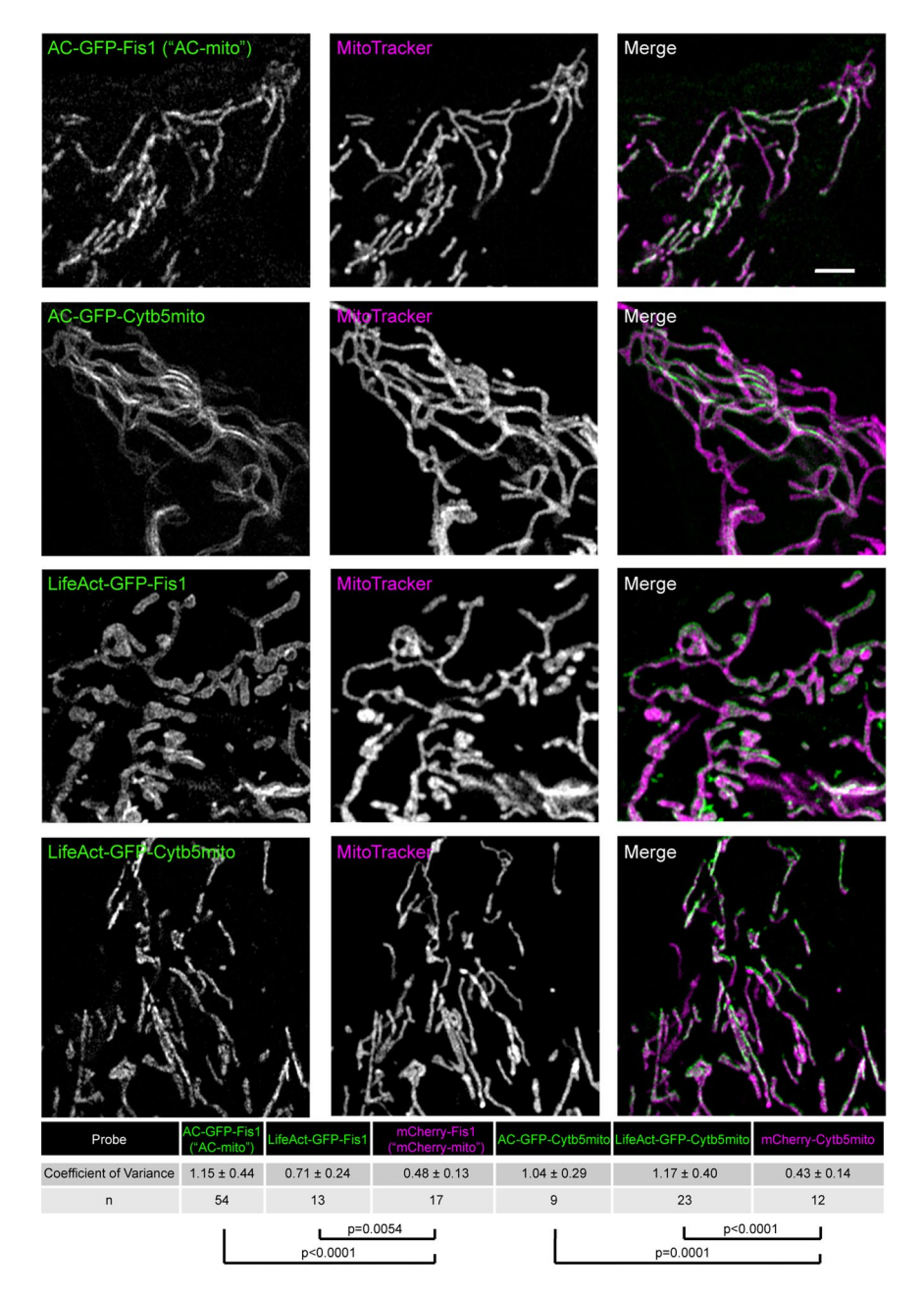


Extended Data Fig. 1 | AC-ER accumulates alongside mitochondria. Left: five high magnification examples of AC-ER accumulating specifically alongside mitochondria are shown. Note that the mCherry-ER control probe does not specifically accumulate in these regions. The degree of correlation with the MitoTracker channel (Mander's correlation coefficient) is shown below each example for both the AC-ER and mCherry control probes. Scale bar: 1 μm. Right: three low magnification examples are shown. Maximum intensity projections are shown. Scale bars: 5 μm. These results were reproducible across 21 independent experiments.

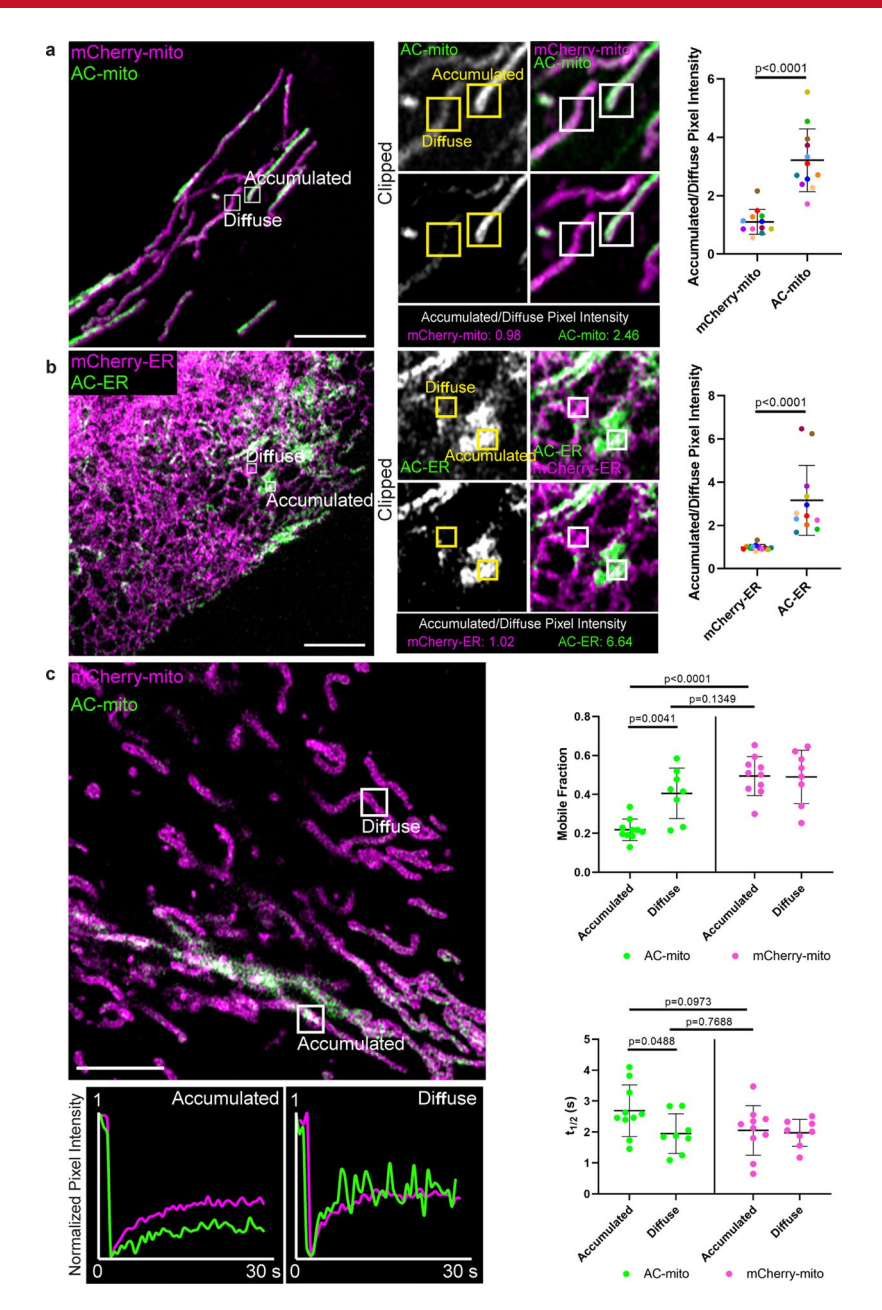


Extended Data Fig. 2 | AC probes provide higher sensitivity and specificity for imaging sub-organellar F-actin accumulation. a) Maximum projection of cells stained with phalloidin and MitoTracker do not show obvious sites of accumulation of actin on mitochondria. Scale bar: 10µm. These results were reproducible across 12 independent experiments. b) Maximum projection of cells expressing an ER marker counterstained with phalloidin do not show obvious accumulation of actin on any specific region of the ER. Scale bar: 10µm. These results were reproducible across 12 independent experiments. c) Expression of AC probes does not alter actin accumulation on mitochondria or the ER. Left graph: HeLa cells were either not transfected or transfected with AC-mito, then stained with MitoTracker and phalloidin. Pearson's correlation coefficient between MitoTracker and phalloidin was determined for each condition. Right graph: HeLa cells were either transfected with mCherry-ER only or cotransfected with mCherry-ER and AC-ER, then stained with phalloidin. Pearson's correlation coefficient between mCherry-ER and phalloidin was determined for each condition. N = 10 cells per condition. P-values determined by two-tailed Welch's t-test. d) Quantification of the percentage of mitochondria or ER overlapped by AC probes, mCherry-tagged control probes, or F-actin probes. Our AC probes display more specific labeling compared to their corresponding controls or pan-actin probes. Quantification of overlap was carried out as displayed in E and described under Methods. Mitochondria overlap: AC-mito: n = 53 cells, AC-ER: n = 76 cells, mCherry-ER: n = 71 cells, F-actin: n = 26 cells. ER overlap: AC-mito: n = 20 cells, AC-ER: n = 73 cells, mCherry-mito: n = 71 cells, F-actin: n = 18 cells. P-values determined by two-tailed Welch's t-test. e) An example of a HeLa cell expressing AC-mito and stained with MitoTracker and phalloidin. Scale bar: 10µm. The top row shows standard images of the cell. The center row shows the corresponding mitochondrial area in magenta and phalloidin or AC-mito area in green. Areas of overlap are shown in white and quantified. The lower left panel displays the area of overlap between mitochondria and phalloidin in cyan and the area of overlap between mitochondria and AC-mito in yellow. The area of overlap between the two is shown in white and quantified. The lower right panel summarizes the qunatification for this example. Green: percentage of mitochondria overlapped by phalloidin or AC-mito. Cyan: percentage of mitochondria overlapped by only phalloidin. This is the proportion of non-specific phalloidin overlap. Yellow: percentage of mitochondria overlapped by only AC-mito. This represents the proportion of actin that phalloidin lacks the sensitivity to detect. White: percentage of mitochondria overlapped by both phalloidin and AC-mito. These results were reproducible across 12 independent experiments. f) Further quantification of E across multiple cells either transfected with AC-mito and labelled with MitoTracker and phalloidin (left graph) or co-transfected with AC-ER and mCherry-ER and labelled with phalloidin (right graph). Averages and standard deviation are shown. N = 10 cells per condition. P-values determined by the two-tailed ratio paired t-test.

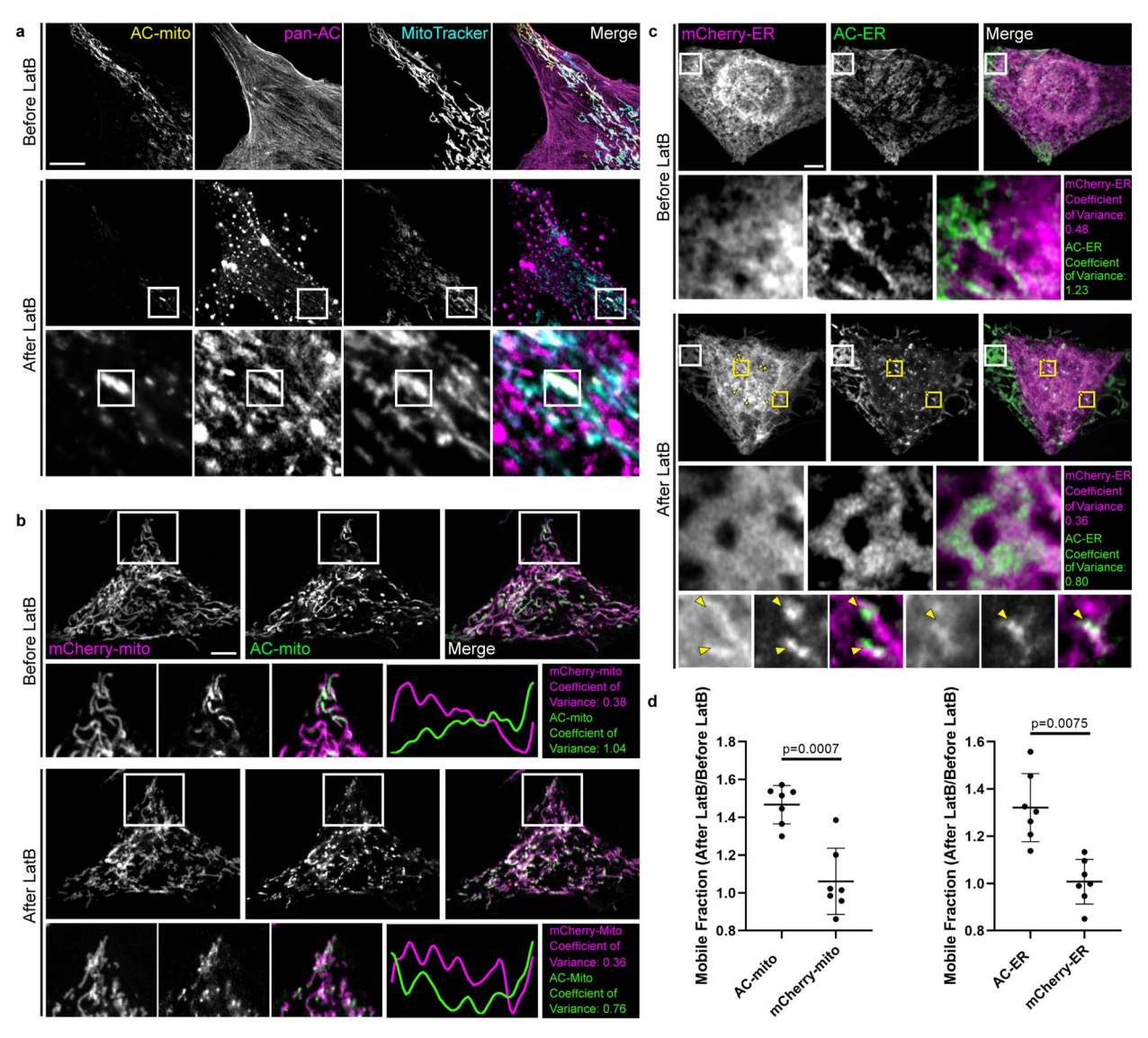
Extended Data Fig. 3 | AC-mito expression does not alter endogenous Fis1 localization to mitochondria. Maximum projection of cells expressing AC-mito and non-transfected cells show similar levels of endogenous anti-Fis1 immunofluorescence. Note that the anti-Fis1 antigen is the Fis1 N-terminus, which is not present in the AC-mito protein, which contains only the C-terminus of Fis1. Scale bar: 20 μm. These results were reproducible across 2 independent experiments.



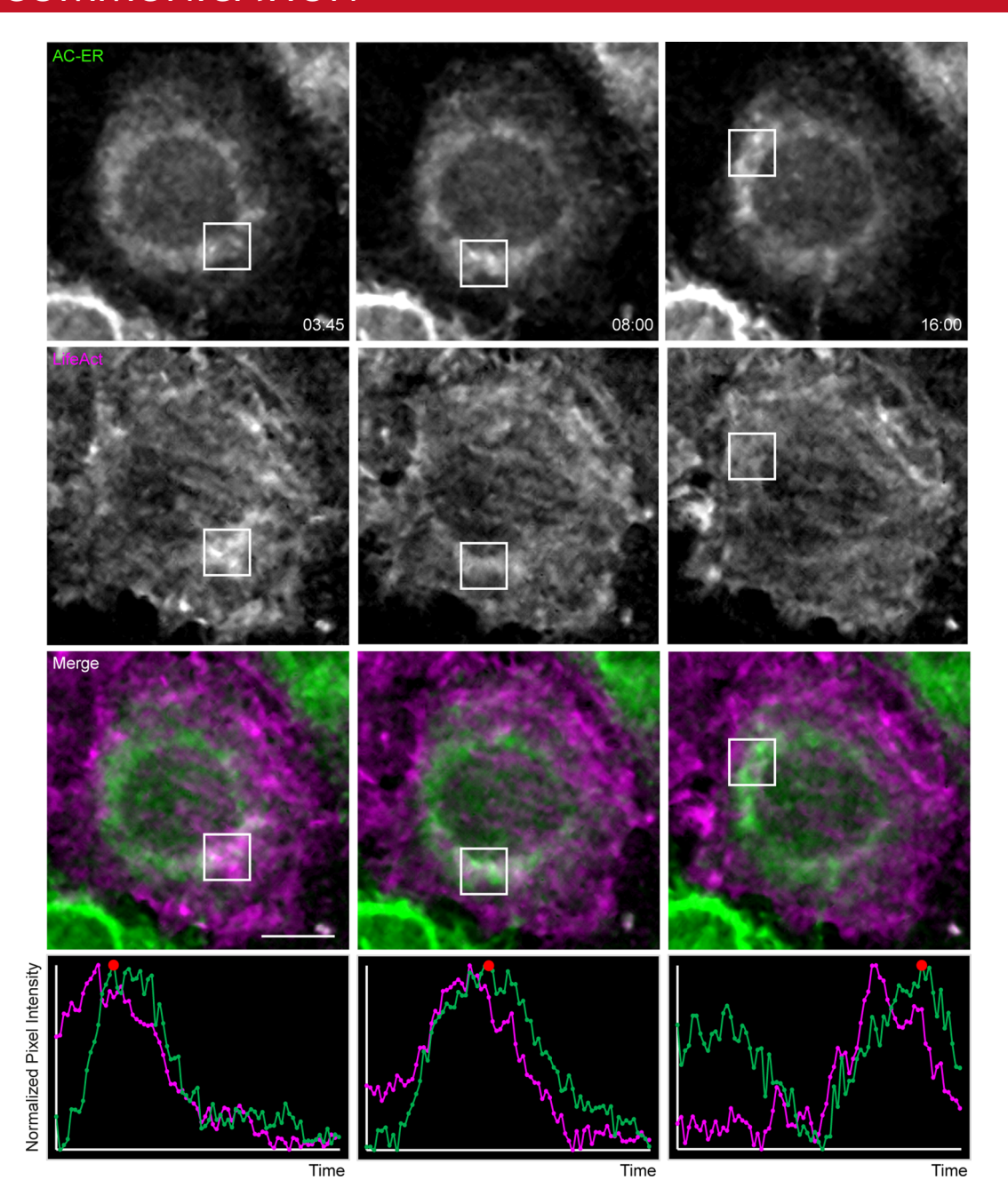
Extended Data Fig. 4 | Alternate membrane-targeting and actin-binding motifs yield similar results. Switching the actin nanobody motif with LifeAct (Fis1-LifeAct-GFP) yields similarly increased accumulation compared to control constructs as quantified by the coefficient of variance. Switching the Fis1 mitochondrial outer membrane targeting sequence for Cytb5mito (Cytb5mito-AC-GFP) also yields similar results. Scale bar: $5 \mu m$. The table displays the degree of accumulation as quantified by the average coefficient of variance (standard deviation/mean pixel intensity in the mitochondrial region) \pm the standard deviation for each probe compared to control probes. N indicates the number of cells analyzed. P-values determined by two-tailed Welch's t-test. These results were reproducible across 7 independent experiments.



Extended Data Fig. 5 | Comparison of AC probe dynamics in "accumulated" vs. "diffuse" regions. a) Example of a cell containing regions with accumulated vs. diffuse AC probe localization. Regions with AC-mito accumulation ("Accumulated") and without AC-mito accumulation ("Diffuse") are indicated. Panels in the lower row ("Clipped") display thresholded AC-mito signal (displaying only the top 25% signal) while the top row displays the same region without thresholding. Scale bar: $5 \mu m$. The mean pixel intensity in boxed regions was determined for AC-mito and the mCherry-mito control probe and the ratio was calculated (mean pixel intensity in accumulated region/mean pixel intensity in diffuse region). The results for the example shown are displayed below the panels and quantification across multiple cells (n=12 cells) is displayed in the scatter plot. Each dot color corresponds to an individual region in which pixel intensity was measured. P-values determined via a two-tailed ratio paired t-test. These results were reproducible across 9 independent experiments. b) Example of AC-ER accumulation. Same as A, showing results for AC/mCherry-ER. c) AC-mito and mCherry-mito have similar mobility in diffuse regions. FRAP was performed on the indicated accumulated and diffuse regions. Fluorescence recovery over time for the example shown is displayed beneath the image. Quantification of the mobile fraction (top scatter plot) and $t_{1/2}$ (bottom scatter plot) across multiple cells is also displayed. Accumulated regions: n=10 cells, diffuse regions: n=8 cells. P-values determined by two-tailed Welch's t-test. These results were reproducible across 3 independent experiments.

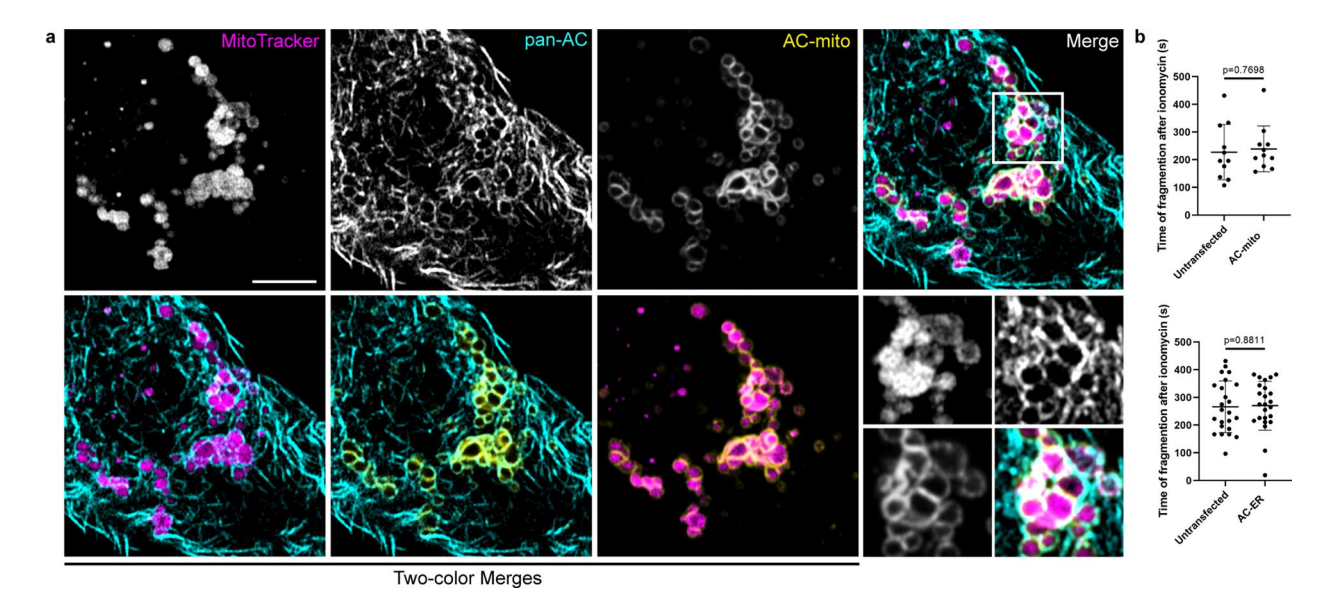


Extended Data Fig. 6 | Actin depolymerization destroys AC-mito and AC-ER accumulation. a) U2OS cells stained with MitoTracker and expressing AC-mito and pan-AC (cytoplasmic AC-tagRFP) were imaged before and after treatment with 2 µM Latrunculin B (LatB) for 30 minutes. After LatB treatment, AC-mito displayed significantly reduced accumulation at specific regions on mitochondria. This loss of accumulation was observed in all cells imaged after treatment with LatB or Cytochalasin D (n = 6 cells). The magnified images in the bottom row show an example of LatB treatment causing actin aggregates which colocalize with AC-mito. Maximum intensity projections are shown. Scale bar: 5 µm. These results were reproducible across 5 independent experiments. b) HeLa cells co-expressing AC-mito and the mCherry-mito control probe before and after treatment with LatB including example insets showing loss of AC-mito accumulation following LatB treatment. The yellow line in the merged inset indicates the area used to generate the line scan. The coefficient of variance was calculated before and after LatB treatment in the boxed region as described under Methods. Scale bar: 5 µm. These results were reproducible across 5 independent experiments. c) HeLa cells co-expressing AC-ER and the mCherry-ER control probe before and after treatment with LatB. The white box marks an area where AC-ER accumulation is lost following LatB treatment. The coefficient of variance for mCherry/ AC-ER was calculated before and after LatB treatment in the white boxed region. Yellow arrows label areas of mCherry/AC-ER aggregation that result from LatB treatment. Higher magnification versions of some of these regions (marked by the yellow boxes) are shown in the bottom row. Scale bar: 5 µm. These results were reproducible across 5 independent experiments. d) FRAP-based quantification of mobile fractions before and after LatB treatment. FRAP was performed on cells co-expressing the mCherry-mito control probe and AC-mito (left graph) or the mCherry-ER control probe and AC-ER (right graph) before and after treatment with LatB. The mobile fraction of each probe was calculated and is displayed as a ratio of the mobile fraction after LatB treatment/the mobile fraction before LatB treatment. The AC probe mobility is increased following LatB treatment while the mobility of the corresponding mCherry control probes is unchanged. N = 7 cells per condition. P-values determined by two-tailed ratio paired t-test. These results were reproducible across 3 independent experiments.

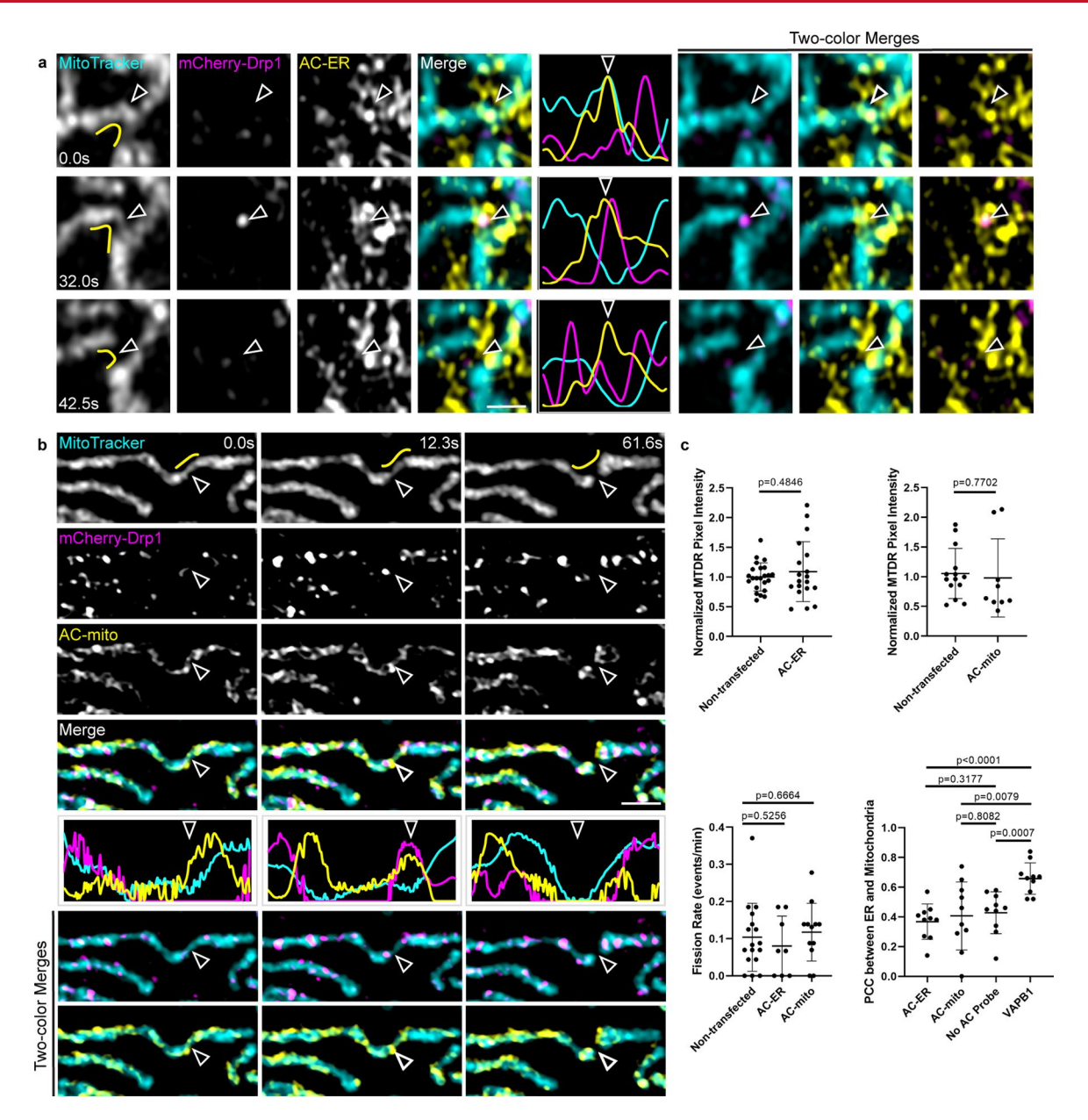


Extended Data Fig. 7 | AC-ER dynamically co-accumulates with F-actin during actin wave cycling. Actin waves were imaged in HeLa cells co-expressing AC-ER and the F-actin marker LifeAct. Boxes mark regions of LifeAct accumulation at different timepoints. Graphs displaying normalized pixel intensity over time in the boxed regions are displayed as insets. This figure represents chosen timepoints from Supplementary Videos 8 and 9. The actin wave dynamics are much more easily visualized in the movies. Scale bar: $5 \mu m$. These results were reproducible across 4 independent experiments.

BRIEF COMMUNICATION

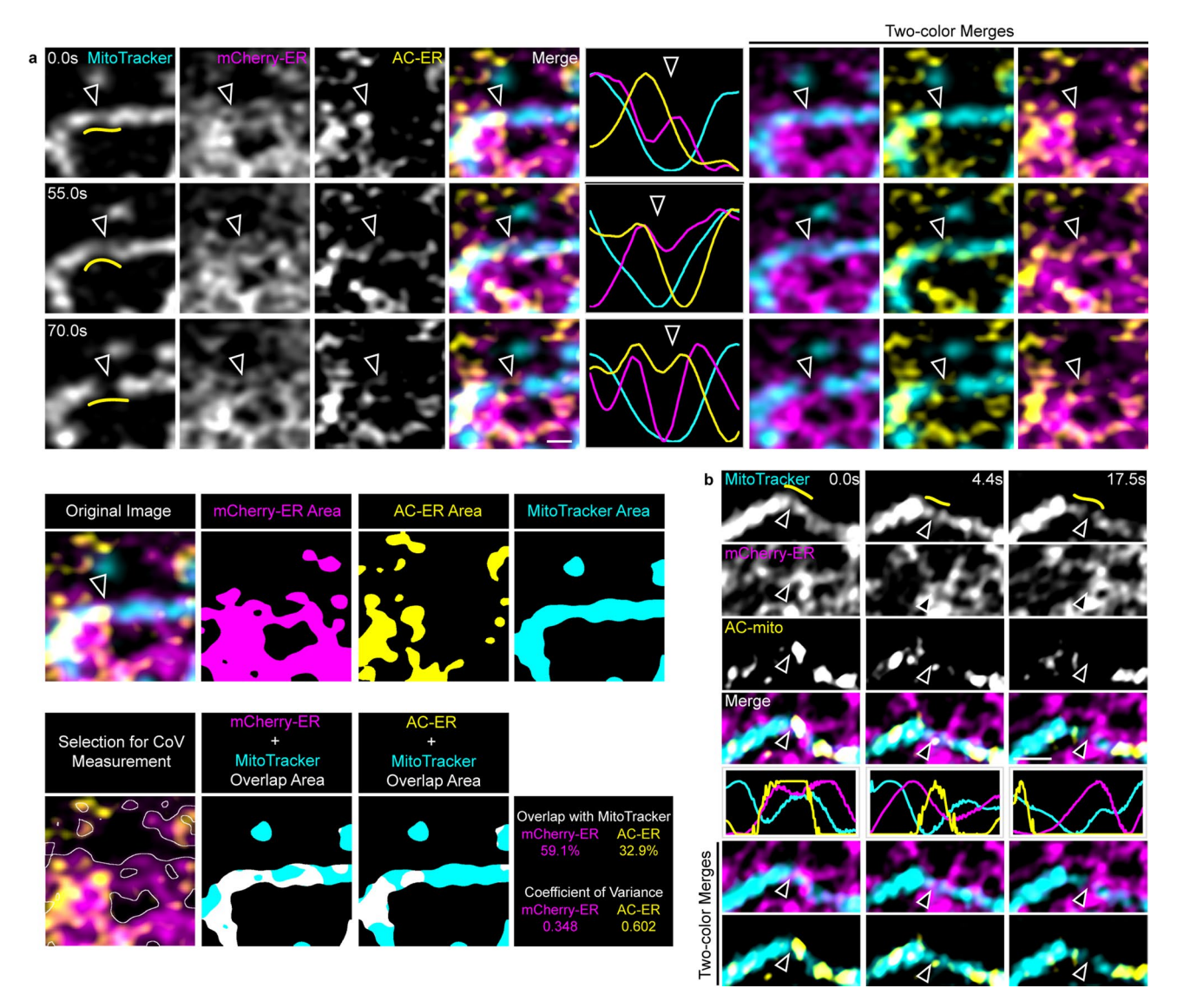


Extended Data Fig. 8 | Impact of ionomycin treatment on cells expressing AC probes. a) HeLa cells stained with MitoTracker and expressing AC-mito and pan-AC (cytoplasmic AC-tagRFP) were treated with 10 μ M ionomycin for 10 minutes. Fragmented mitochondria surrounded by both pan-AC and AC-mito can be visualized. Scale bar: 5 μ m. These results were reproducible across 5 independent experiments. b) HeLa cells expressing AC-mito or AC-ER and counterstained with MitoTracker were treated with 10 μ M ionomycin and imaged for 10 minutes. The time after ionomycin addition when mitochondrial fragmentation became evident was recorded for each cell. Cells from the same field displaying no AC-mito or AC-ER signal were considered untransfected. AC-mito: n= 11 cells, AC-ER: n = 24 cells. P-values determined by two-tailed Welch's t-test.



Extended Data Fig. 9 | Mitochondria- and ER-associated actin accumulates during Drp1-mediated mitochondrial fission. a) AC-ER accumulates prior to Drp1-mediated fission. AC-ER accumulation is evident prior to Drp1 recruitment and mitochondrial fission. Hollow arrows mark the location of mitochondrial fission. Yellow lines in the left column mark the area used to generate the line scans. Scale bar: 1 μm. These results were reproducible across 8 independent experiments. b) AC-mito accumulates prior to Drp1-mediated fission. Same as A with cells expressing AC-mito instead of AC-ER. c) Expression of AC probes does not alter mitochondrial membrane potential, mitochondrial fission rate, or ER-mitochondria contact sites. Top graphs: the pixel intensity of MitoTracker Deep Red (MTDR) was measured in cells that were not transfected vs. neighboring cells expressing AC-mito/ER and normalized as described under Methods. Left graph: non-transfected: n = 23 cells, AC-ER: n = 19 cells. Right graph: non-transfected: n = 14 cells, AC-mito: n = 9 cells. P-values determined by two-tailed Welch's t-test. Bottom left graph: the number of fission events were counted in cells that were not transfected or in cells expressing AC-mito/ER. Non-transfected: n = 17 cells, AC-ER: n = 8 cells, AC-mito: n = 12 cells. P-values determined by two-tailed Welch's t-test. Bottom right graph: HeLa cells were transfected with mCherry-ER alone "No AC Probe", AC-ER+mCherry-ER "AC-ER", AC-mito+mCherry-ER "AC-mito, or VAPB1-Halo+mCherry-ER "VAPB1" (positive control for changing ER-mitochondria contacts) and counterstained with MitoTracker. A region of the cell was selected as described under Methods and Pearson's correlation coefficient between MitoTracker and mCherry-ER was determined. N = 10 cells per condition. P-values determined by two-tailed Welch's t-test.

BRIEF COMMUNICATION



Extended Data Fig. 10 | Mitochondria- and ER-associated actin accumulates during ER-mediated mitochondrial fission. a) AC-ER specifically accumulates at fission sites prior to ER-mediated fission. AC-ER accumulation is evident during ER-mediated mitochondrial fission. Hollow arrows mark the location of mitochondrial fission. Yellow lines in the left column mark the area used to generate the line scans. Scale bar: 1 µm. Example images of the areas used to determine the degree of MitoTracker overlap and coefficient of variance for mCherry/AC-ER and the resulting values are also shown. These results were reproducible across 19 independent experiments. **b)** AC-mito accumulates prior to ER-mediated fission. Same as A with cells expressing AC-mito instead of AC-ER.

nature research

Corresponding author(s):	Uri Manor
Last updated by author(s):	Jul 3, 2020

Reporting Summary

Nature Research wishes to improve the reproducibility of the work that we publish. This form provides structure for consistency and transparency in reporting. For further information on Nature Research policies, see our <u>Editorial Policies</u> and the <u>Editorial Policy Checklist</u>.

\sim				٠	
⋖.	t a	t١	st	Ή.	\sim

For	all statistical analyses, confirm that the following items are present in the figure legend, table legend, main text, or Methods section.
n/a	Confirmed
	The exact sample size (n) for each experimental group/condition, given as a discrete number and unit of measurement
	A statement on whether measurements were taken from distinct samples or whether the same sample was measured repeatedly
	The statistical test(s) used AND whether they are one- or two-sided Only common tests should be described solely by name; describe more complex techniques in the Methods section.
X	A description of all covariates tested
X	A description of any assumptions or corrections, such as tests of normality and adjustment for multiple comparisons
	A full description of the statistical parameters including central tendency (e.g. means) or other basic estimates (e.g. regression coefficient AND variation (e.g. standard deviation) or associated estimates of uncertainty (e.g. confidence intervals)
	For null hypothesis testing, the test statistic (e.g. <i>F</i> , <i>t</i> , <i>r</i>) with confidence intervals, effect sizes, degrees of freedom and <i>P</i> value noted <i>Give P values as exact values whenever suitable.</i>
\boxtimes	For Bayesian analysis, information on the choice of priors and Markov chain Monte Carlo settings
X	For hierarchical and complex designs, identification of the appropriate level for tests and full reporting of outcomes
	Estimates of effect sizes (e.g. Cohen's <i>d</i> , Pearson's <i>r</i>), indicating how they were calculated
	Our web collection on <u>statistics for biologists</u> contains articles on many of the points above.

Software and code

Policy information about <u>availability of computer code</u>

Data collection ZEISS 880 LSM Airyscan confocal system

Data analysis

Images were Airyscan processed using the autofilter 2D-SR settings in Zen Blue (ZEISS) or the auto-filter 3D settings in Zen Black (ZEISS). All images were post-processed and analyzed using Imaris v9.5.1 (BITPLANE) and Fiji v2.0.0-rc-69/1.5p software. The IsoData algorithm used for thresholding is part of Fiji and referenced in the Methods section. All statistical analysis was done using GraphPad Prism v8.4.3.

For manuscripts utilizing custom algorithms or software that are central to the research but not yet described in published literature, software must be made available to editors and reviewers. We strongly encourage code deposition in a community repository (e.g. GitHub). See the Nature Research guidelines for submitting code & software for further information.

Data

Policy information about <u>availability of data</u>

All manuscripts must include a data availability statement. This statement should provide the following information, where applicable:

- Accession codes, unique identifiers, or web links for publicly available datasets
- A list of figures that have associated raw data
- A description of any restrictions on data availability

Source data for Figures 1-3 and Extended Data Figures 2 and 4-10 containing raw data for all quantifications are provided with the paper. The original imaging data used to generate the raw data and all the presented figures and videos are available from _.

Fie	ld-	SD	ecif	ic	rep	ort	ing
		7	C 011	. •	. – –	0. 0	c

<u> </u>	ne below that is the best fit for your research. If you are not sure, read the appropriate sections before making your selection.		
∑ Life sciences	Behavioural & social sciences Ecological, evolutionary & environmental sciences		
For a reference copy of t	he document with all sections, see <u>nature.com/documents/nr-reporting-summary-flat.pdf</u>		
Life scier	nces study design		
All studies must dis	close on these points even when the disclosure is negative.		
Sample size	e size was determined by counting cells or cellular events (i.e. organelle fission or constriction events) with n being the number of cells ular events observed within a given condition. The sample sizes used produced statistically significant results.		
Data exclusions	Live-cell imaging data were only excluded in instances where the cell died during imaging or moved significantly out of focus such that experimental conclusions could not be clearly interpreted. No other data were excluded.		
Replication	All attempts at replication were successful. All experiments were independently repeated at least twice and often much more than twice. The specific number of independently repeated experiments is provided in the figure legends.		
Randomization	Randomization was not relevant in this study because all imaging experiments where performed using the same experimental conditions.		
Blinding	Blinding was not conducted as all results were inherently objective and quantitatively measured.		
system or method list Materials & exp	on from authors about some types of materials, experimental systems and methods used in many studies. Here, indicate whether each material red is relevant to your study. If you are not sure if a list item applies to your research, read the appropriate section before selecting a response. Derimental systems Methods		
n/a Involved in th			
Antibodies ChIP-seq			
Eukaryotic cell lines Flow cytometry Ralaeontology and archaeology MRI-based neuroimaging			
Animals and other organisms			
	earch participants		
Clinical data			
Dual use re	esearch of concern		
Antibodies			
Antibodies used	anti-Fis1 antibody, made by Prestige Antibodies Powered by Atlas Antibodies, Sigma-Aldrich, catalog #: HPA017430		
Validation	The anti-Fis1 antibody was validated by the vendor via Western blot, immunohistochemistry, and immunofluorescence staining in 3 different human cell lines and tissues.		
Eukaryotic c	ell lines		

Policy information about <u>cell lines</u> Cell line source(s) U2OS, Hap1, and HeLa cell lines were obtained from the ATCC. HeLa cells stably expressing LifeAct-mCherry were from the Wedlich-Soldner lab as referenced under Methods. Cell lines were authenticated by ATCC but not by us. Authentication Mycoplasma contamination All cell lines tested negative for mycoplasma contamination Commonly misidentified lines No commonly misidentified cell lines were used in this study. (See ICLAC register)